IOP Publishing and International Atomic Energy Agency Nuclear Fusion
Nucl. Fusion **51** (2011) 103022 (6pp) doi:10.1088/0029-5515/51/10/103022

Pedestal characterization and stability of small-ELM regimes in NSTX

A.C. Sontag[1], J.M. Canik[1], R. Maingi[1], J. Manickam[2], P.B. Snyder[3], R.E. Bell[2], S.P. Gerhardt[2], S. Kubota[4], B.P. LeBlanc[2], D. Mueller[2], T.H. Osborne[3] and K.L. Tritz[5]

[1] Oak Ridge National Laboratory, Box 2008, Oak Ridge, TN 37831, USA
[2] Princeton Plasma Physics Laboratory, PO Box 451, Princeton, NJ 08543, USA
[3] General Atomics, San Diego, CA 92186-5608, USA
[4] Institute of Plasma and Fusion Research, University of California, Los Angeles, CA 90095, USA
[5] Physics and Astronomy Department, John's Hopkins University, Baltimore, MD 21218, USA

E-mail: sontagac@ornl.gov

Received 13 January 2011, accepted for publication 11 July 2011
Published 2 September 2011
Online at stacks.iop.org/NF/51/103022

Abstract
NSTX has observed transition to a desirable small-ELM regime (called type-V), in which the stored energy loss per ELM is less than 1%, by stabilizing type-I ELMs. This regime is accessed in a lower single null configuration with increased edge collisionality ($\nu^* > 1$). Coincident with the transition to this regime, a low-frequency (<10 kHz) $n = 1$ mode is observed at the plasma edge in magnetic and soft x-ray diagnostics, with harmonics up to $n = 6$ observed in some cases. Low-level density fluctuations associated with this mode are observed using microwave reflectometry, but there is no evidence that the mode is providing sufficient transport to stabilize the type-I ELMs. This mode rotates in the electron diamagnetic direction and has shown a phase inversion on USXR channels, indicating that it is resistive in nature. Discharges with type-V and type-I ELMs are both calculated to be on the peeling unstable side of the peeling–ballooning stability curve, with the type-V case at higher normalized pressure gradient and closer to the ballooning stability boundary.

(Some figures in this article are in colour only in the electronic version)

1. Introduction

Predictable and reliable access to high confinement mode (H-mode) regimes with small or no edge-localized modes (ELMs) is highly desirable for future large experiments such as ITER to ensure adequate survivability of the first wall [1]. To avoid unacceptable erosion of plasma-facing components in ITER, the maximum allowable drop in the plasma stored energy is 1% per ELM [1]. A small-ELM operating regime (called type-V ELMs) has been observed on the National Spherical Torus Experiment (NSTX) [2] that is characterized by ELMs that drop the stored energy by less than 1% [3, 4]. This work is focused on understanding the physics allowing access to this operating regime in order to determine if it will be accessible in future devices that will operate with much higher magnetic fields and lower collsionality.

The type-V ELM operating regime is accessed in NSTX by stabilizing type-I ELMs. Coincident with the transition to this regime, a low-frequency ($f < 10$ kHz) edge instability is observed. This instability is distinguished from the magnetic signature of the type-V ELMs reported in previous publications [3, 4] by being a long-lived, coherent mode at higher frequency. The magnetic signature shown previously was composed of discrete events with a single cycle lasting approximately 1.5 ms, and only one–two cycles being observed. The mode being discussed in this work is coherent, typically observed at 2–5 kHz and lasts for several hundred milliseconds. This mode is observed in all shots with type-V ELMs that have been examined to date, including the discharges examined in previous publications. The amplitudes of the magnetic perturbations due to this mode are weak in comparison with coexisting core modes, which is probably why they were not reported earlier.

The coincidence of this instability with the stabilization of type-I ELMs in NSTX invites comparison with the edge harmonic oscillation (EHO) that is believed to stabilize type-I ELMs and allow access to quiescent H-mode (QH-mode) at standard aspect ratio [5], as has been observed on DIII-D [6], ASDEX [7], JT-60U [8] and JET [7]. It is possible that the NSTX edge instability is stabilizing the type-I ELMs, but it is also possible that the stabilization of the type-I ELMs allows the growth of the edge instability. Section 2 of this paper will present the observed characteristics of the edge instability on NSTX and how this mode compares with the EHO. Section 3

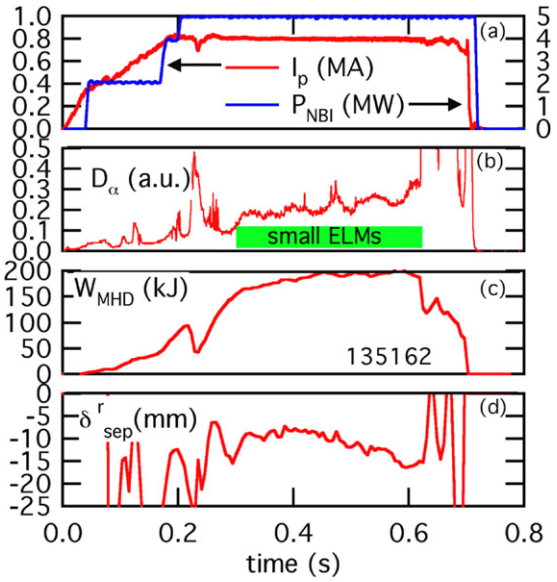

Figure 1. Time evolution of shot 135162 showing a transition to small-ELMs at 0.29 s.

will discuss the plasma characteristics and MHD stability of the type-V ELMy discharges when the edge mode is present. Section 4 will summarize and discuss these results.

2. NSTX edge instability characteristics

The EHO allows access to the QH-mode by providing transport near the edge that is necessary to stabilize the peeling–ballooning modes responsible for ELMs [9], while maintaining good core confinement inside the pedestal. The EHO is hypothesized to be a saturated low-n kink that is destabilized by rotational shear and is accessed at low density and high rotational shear at the plasma edge [9–11]. The conditions required to access the edge instability in NSTX and the effects of this mode on transport are examined here and compared with the EHO.

The time evolution of an NSTX discharge with a transition to small-ELMs and the associated edge instability is shown in figure 1. In this discharge, there are some large ELMs after the plasma current flat-top, then a transition to small-ELMs occurs at 0.29 s as shown in the D_α trace in panel (b). The small-ELMs decrease the plasma stored energy by $<1\%$, i.e. well below the statistical uncertainty in equilibrium reconstructions. In NSTX discharges, transition to the small-ELM regime is associated with a downward biased plasma as evidenced by $\delta_R^{\rm sep} < -5$ mm, which is consistent with previous observations [3] ($\delta_R^{\rm sep}$ is the radial separation of the two separatraces at the outer midplane).

The edge mode coincident with the transition to small-ELMs is observed in the Mirnov coils as well as in ultrasoft x-ray (USXR) emission [12], as shown in panels (a) and (b) of figure 2. The diode array channels are at a single toroidal location and have poloidal lines of sight with tangency radii that extend from the magnetic axis into the scrape-off layer. The diodes are filtered with 10 μm of Be foil, which eliminates low energy radiation from the scrape-off layer and lower pedestal. The mode is observed as low frequency

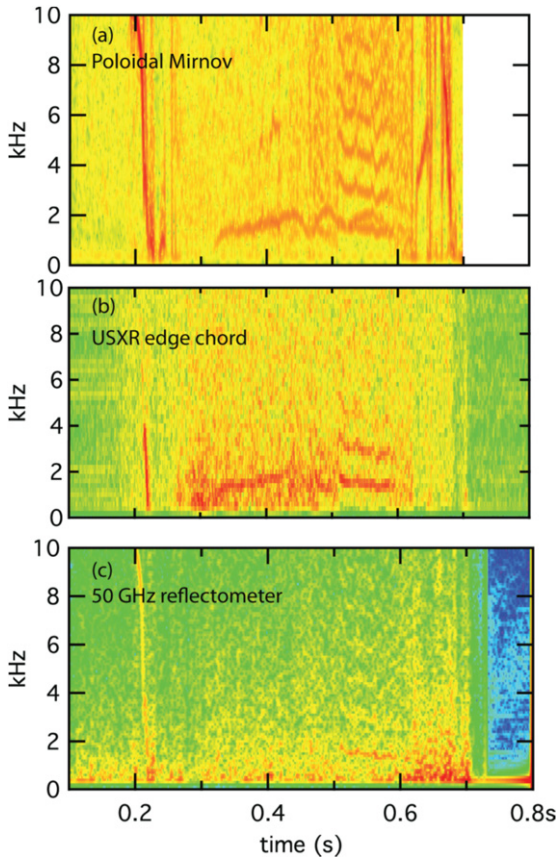

Figure 2. Measurements of an instability near the plasma edge in shot 135162 including (a) a poloidal Mirnov coil, (b) a USXR chord viewing near the plasma edge tangent to the flux surface at $r/a = 0.95$ and (c) a reflectometer channel with a cutoff location near the top of the H-mode pedestal at $r/a = 0.94$.

oscillations that grow most strongly in the USXR channels near the plasma edge starting at approximately 0.29 s (coincident with the transition to small-ELMs). The channel shown in figure 2(b) is the channel with the peak amplitude and is tangent to the flux surface at $r/a = 0.95$. The mode decreases in amplitude moving towards the core, and is detectable as far in as $r/a = 0.8$. The mode is not measured in channels outside of $r/a = 0.95$ because the Be filters cut off the emission from this cold portion of the plasma. For reference, the top of the pedestal is at $r/a = 0.89$ and the bottom is at $r/a = 0.96$.

The measured oscillations are coherent with a fundamental mode at 1–3 kHz that is present throughout the small-ELM period. Higher harmonics are observed after a slight drop in upper triangularity at ~0.47 s, and a second mode with similar frequency appears in the magnetics at ~0.55 s. This second mode is observed in the Mirnov array, but not in the USXR edge channels. This indicates that this second mode is in the scrape-off region where the emission is cut off by the Be filters. This overlapping secondary mode is not commonly observed, and appears to have no affect on the edge, so it will not be discussed further. Toroidal mode analysis of the fundamental mode observed on the Mirnov coils indicates $n = 1$ with the mode propagating counter to the plasma current, in the electron diamagnetic drift direction. This is in contrast to the EHO, which propagates in the ion diamagnetic drift direction, suggesting that this mode is not the same type of mode as the

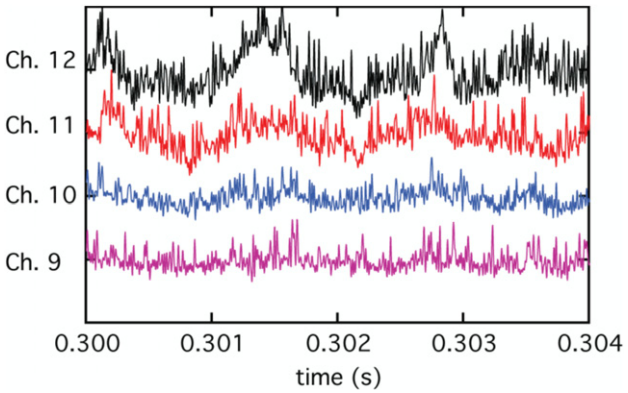

Figure 3. USXR diode array signals in four channels viewing near the plasma edge with 10 μm Be filters and frequency filtered to 0.5–80 kHz. These channels are tangent to the flux surfaces at $r/a = 0.95$ (Ch. 12), $r/a = 0.87$ (Ch. 11), $r/a = 0.8$ (Ch. 10) and $r/a = 0.73$ (Ch. 9).

EHO. The toroidal mode numbers of the higher harmonics are integer multiples of the fundamental mode. While the higher harmonics have been observed in some cases such as this one, they are not routine, as they are for the EHO [13].

Density fluctuations measured with an O-mode reflectometer are shown in figure 2(*c*). This channel has a frequency of 50 GHz, which places the cutoff layer in the steep gradient region of the pedestal at $r_{\rm cutoff}/a = 0.94$. These measurements show weak density fluctuations at the same frequencies as the observed modes. Initial TRANSP [14] modelling of discharges both with and without the edge mode show little to no difference in the single-fluid effective transport coefficient near the edge. It should be noted that the TRANSP modelling does not account for particle sources and sinks at the plasma edge, so there is great uncertainty outside of $\rho_{\rm pol} = 0.85$. These two discharges have similar time evolution of most global parameters, and their characteristics are discussed in greater detail in section 3. Data indicate that the edge ion density gradient is reduced in the case with the edge mode; however, more detailed modelling, including particle sources and sinks is required to determine if this instability is providing the particle transport required to stabilize the peeling–ballooning modes, as is suspected with the EHO.

The oscillations observed on the USXR array initially grow in-phase, as shown in figure 3. This figure shows the time evolution of four USXR channels near the edge for shot 135162, filtered to a frequency window of 500 Hz–80 kHz. These channels are tangent to the flux surfaces at $r/a = 0.95$ (Ch. 12), $r/a = 0.87$ (Ch. 11), $r/a = 0.8$ (Ch. 10), and $r/a = 0.73$ (Ch. 9). The next channel with a line of sight at larger tangency radius (Ch. 13) sees no signal because the beryllium filters cut off all of the light from the low-temperature scrape-off layer plasma. The large amplitude slow oscillations (one half period prominent in channel 12 from 0.301 s to 0.302 s) are the coherent oscillations due to the edge mode. The observed mode amplitude peaks near the plasma edge and decreases in the channels viewing closer to the magnetic axis. The mode is not observed in channels closer to the magnetic axis than channel 9. In this case, the oscillations are all in phase, but in some cases, an inversion is observed between channels 11 and 12 at later times (50–100 ms after the initial mode appearance). The outer edge of the plasma is fixed, but the q-profile is evolving during this time with the edge-q slowly increasing, which moves the mode rational surface into a smaller major radius. Since a phase inversion is sometimes observed and the farthest edge channels are cutoff, it is likely that this is a resistive mode. This is also consistent with the observed propagation in the electron diamagnetic direction. These oscillations persist throughout the small-ELM period. After 0.5 s, multiple harmonics can be observed with frequencies corresponding to integer multipliers of the lowest frequency mode, which is similar to observations of the EHO. It should be noted, however, that the mode frequencies are much lower for both the fundamental and harmonics, as compared with the EHO.

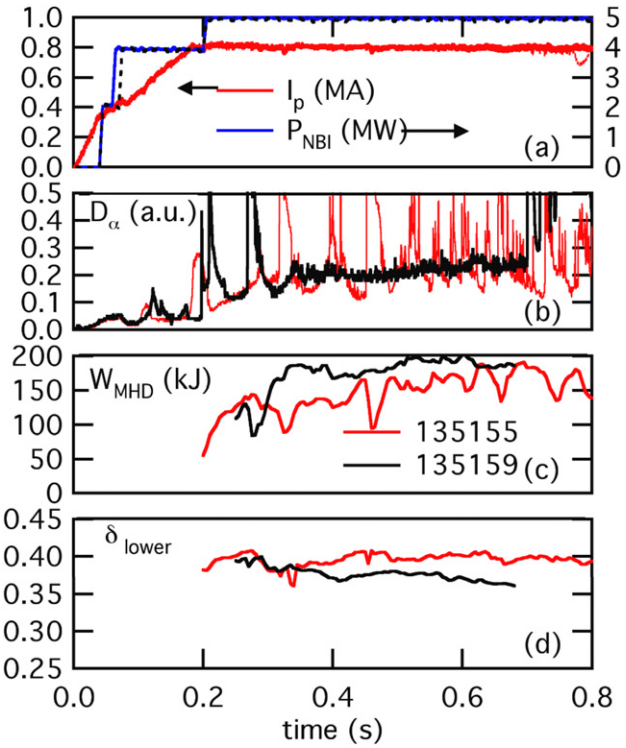

Figure 4. Time evolution of two discharges with similar global plasma parameters but different ELM characteristics. The control shot (red in panels (*b*)–(*d*)) has type-I ELMs. The second shot (black in panels (*b*)–(*d*)) transitions to a small-ELM regime coincident with a programmed change in triangularity at 0.3 s.

3. Plasma characteristics and MHD stability

A comparison of two similar discharges, one with large type-I ELMs and one with small type-V ELMs, illustrates the advantages of operating in a small-ELM regime and provides an opportunity to determine the plasma conditions required for a transition to this regime. The time evolution for two shots with similar time evolution of global plasma parameters, except for a programmed change in triangularity at 0.3 s, is shown in figure 4. The control discharge (135155) has large type-I ELMs throughout the discharge, while the second discharge (135159) transitions to a small-ELM regime soon after the decrease in triangularity. The edge mode discussed in section 2 is observed in the small-ELM discharge but not in the control discharge. The small-ELM discharge has higher stored

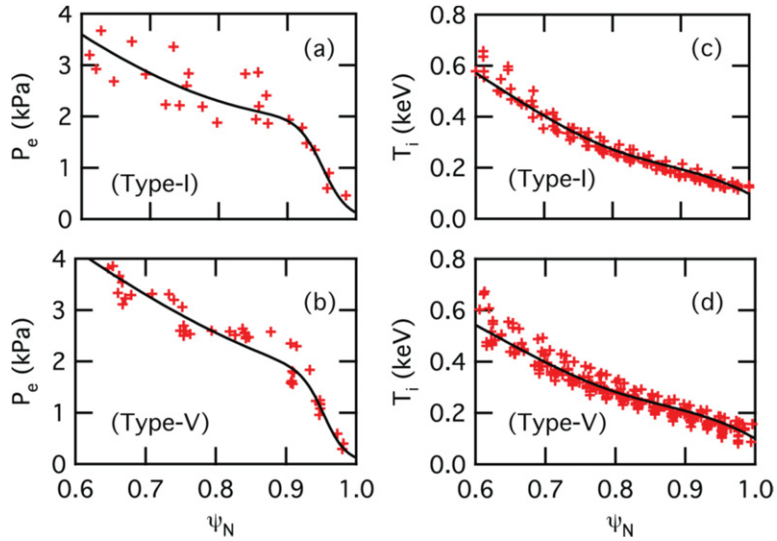

Figure 5. Time-averaged, flux-surface mapped electron pressure and ion temperature data (red crosses) for a 150 ms window and a function (black line) that is fit to the data points. The modified hyperbolic tangent function is fit to the electron pressure data while a spline function is fit to the ion temperature. The type-I case is shown in (*a*) and (*c*), where only profile data from the last 50% of the ELM cycle is included. The type-V case is shown in (*b*) and (*d*) using all time points.

energy, without the large fluctuations that occur during the type-I ELM crashes. The location of the plasma boundary is also more stable and the edge temperature and density profiles are relatively stationary in the type-V case, without the cycle of edge pressure buildup and crash associated with type-I ELMs.

An edge profile comparison using time-averaged values of the Thomson scattering [15] and CHERS [16] diagnostic data has been performed for these two shots to determine if the change in profile characteristics going from type-I to type-V ELMs are similar to those associated with access to QH-mode and the EHO at standard aspect ratio. The edge profiles of type-V ELMy discharges have been examined in previous work [4]. However, since that work, five more channels of Thomson scattering data have been added in the pedestal and high resolution CHERS data is now routinely available. The profiles for these discharges were determined using a procedure developed on DIII-D [9, 17], which was not used for previous NSTX studies on type-V ELMs, and is briefly outlined here: (1) reconstruct the MHD equilibrium at the times of Thomson scattering measurements using the EFIT [18] code with magnetic diagnostics for constraint. (2) Map the n_e, T_e, n_i and T_i profiles into normalized flux space. (3) Fit a modified hyperbolic tangent (tanh) function [19] or spline function to the aggregate profile data from a specified time window. (4) Compute the equilibrium using the fit profiles as additional constraints. The Sauter neoclassical model [20] is used to provide an estimate of the edge bootstrap current which is also used as a constraint. This technique of conditional averaging/correlated sampling to determine the edge profiles, in conjunction with five more channels of Thomson scattering in the pedestal region and routine access to high resolution CHERS data, gives greater confidence in the edge profile determination as compared with previous work [4].

The time window between 0.4 s and 0.55 s was used for the profile comparison of the two shots. Only profiles during the final 50% of the ELM cycle were used for the type-I case, while all time points were used for the type-V discharge. An example of the raw data and fitted tanh profiles for the electron pressure is shown in figure 5. In both the type-I case shown in figure 5(*a*) and the type-V case shown in figure 5(*b*), this averaging procedure provides multiple pressure data points in the pedestal region to constrain the functional fit. While there is more scatter in the core, the pedestal data outside of $\psi_N = 0.9$ are well represented by the fit functions. The ion pressure data and the fit spline functions are shown in figures 5(*c*) and (*d*) for the same two shots.

The edge pressure and pressure gradient profiles for these two discharges are shown in figure 6. The electron pressure profiles are nearly identical from the edge through the pedestal as shown in figure 6(*a*). The ion pressure pedestal is shifted inwards and increased in the type-V case as compared with the type-I case, as shown in figure 6(*b*). The shift in ion pressure is due to a decrease in the ion density gradient in the pedestal. This decrease in the ion density gradient is indicative of increased edge transport, which may be due to the edge mode and would be similar to the role of the EHO during QH-mode. The ion pressure at the top of the pedestal is increased from ~0.75 kPa in the type-I case at a normalized flux of 0.98 to ~1 kPa at a normalized flux of 0.95. Since there is no difference in the electron pressure profiles between the two cases, this change in the ion pressure causes a corresponding change in the total pressure profile as shown in figure 6(*c*). As a result, the gradient in the total pressure in the type-I case has a peak near the plasma edge that is not present in the type-V case. A similar inward shift of the total pressure gradient away from the separatrix is believed to result in the stabilization of ELMs in lithiated discharges [21]. It should be noted that these profiles are only as accurate as the fits to the time-averaged data and more profile comparison cases are required to determine if this inward shift in the pressure gradient is stabilizing the ELMs.

There is large uncertainty in the time-averaged profile fits for the toroidal rotation data. For both cases, there is significant uncertainty in the rotation measurement at the edge,

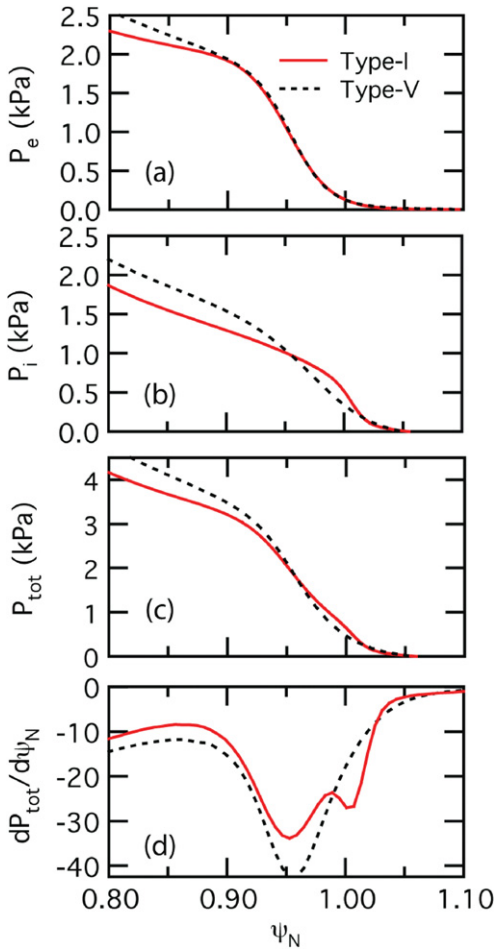

Figure 6. Pressure profiles and total pressure gradient for the type-I (solid red) and type-V (dashed black) cases. Shown are (*a*) the electron pressure, (*b*) the ion pressure, (*c*) the total pressure and (*d*) the gradient in the total pressure.

and the rotation profile evolves significantly over the time-averaging window. Comparison of the single-time toroidal rotation and rotation shear at the top of the pedestal for a larger database of shots during both type-I and type-V ELMs show no correlation with either toroidal rotation or rotation shear and the appearance of the edge mode. The database comparisons show that $\nu^* > 1$ at the top of the H-mode pedestal is required to eliminate type-I ELMs in NSTX, consistent with past observations of type-V ELMs as compared with type-I ELMing discharges [3]. This is shown in figure 7 for the larger database of type-V ELMing discharges. Discharges with type-I ELMs typically have $\nu^* < 1$ during the inter-ELM period as shown in [3]. This figure also demonstrates the requirement that the plasma be biased downwards, as evidenced by the lack of points with $\delta_R^{sep} > -5$ mm.

NSTX is typically on the peeling side of the peeling–ballooning stability curve [21]. The peeling mode is an edge-localized, current-driven external kink, so the increased pedestal collisionality associated with type-V ELMs hints that the mode might be stabilized by the reduction in the pressure-driven current near the edge. Figure 8 shows a comparison of the reconstructed total toroidal current profiles for these two discharges. While the bootstrap current alone is actually increased for the type-V case, there is a slight reduction in

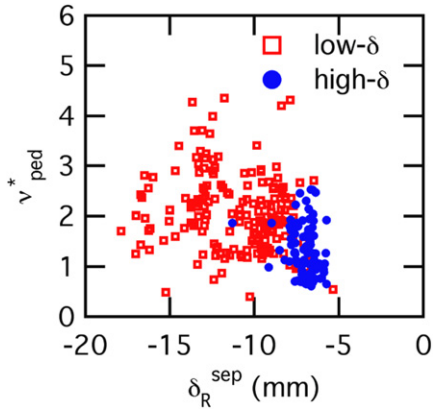

Figure 7. Collisionality at the top of the pedestal and δ_R^{sep} for a large database of type-V ELMing discharges.

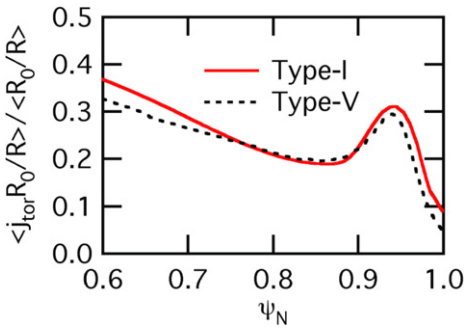

Figure 8. Reconstructed edge current profiles for two discharges. One with type-I ELMs (solid red) and one with type-V ELMs (dashed black).

the total toroidal current in the type-V case as compared with the type-I case. Since these profiles are reconstructed and not measured though, these variations are within the experimental error and are not conclusive. If the plasma is marginally stable to peeling–ballooning modes, even a slight current reduction such as that shown in these profiles can move the plasma into the stable region of stability space. These data are not sufficient to conclude that the reduction in edge current is the mechanism responsible for the stabilization of the type-I ELMs, but it is one possible scenario.

Ideal MHD stability analysis using these profiles has been performed using both the ELITE [22, 23] and PEST [24] stability codes. PEST calculations indicate $n = 3$–5 are the most unstable modes. Figure 9 shows the ELITE peeling–ballooning stability calculations for $n = 3$, 6, 9, 12 and 15 in the type-I case. The red region in the upper left portion of the figure represents the unstable portion of the stability space. The box represents the operating point with the cross indicating the confidence in the pressure gradient and edge current. The stability boundary of $\gamma/(\omega_*/2) = 0.1$ is consistent with the calculated ELM stability of previous NSTX discharges [21]. This case is on the boundary that denotes the peeling side of the stability curve with $n = 3$ being the most unstable mode. Being on the peeling side of the stability curve is typical for NSTX discharges due to the strong bootstrap current drive at low aspect ratio as compared with standard aspect ratio. The high shaping of NSTX discharges is stabilizing to ballooning modes [25], which results in the ballooning stability boundary being off the right-hand side of figure 9.

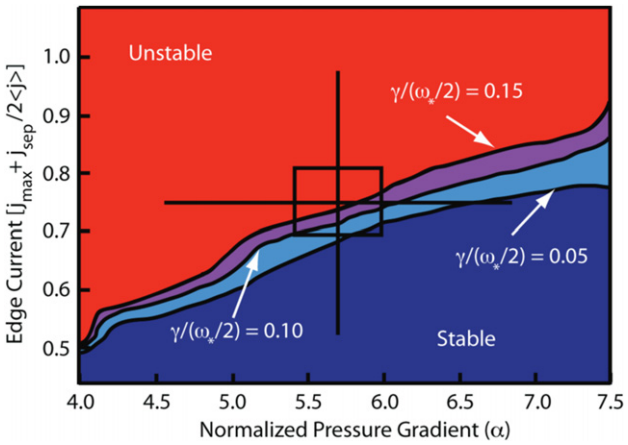

Figure 9. Peeling–ballooning stability diagram as calculated by the ELITE code for shot 135155 during the type-I ELMy phase. The boundary of $\gamma/(\omega_*/2) = 0.10$ has been found to be the type-I ELM stability boundary in previous studies on NSTX .

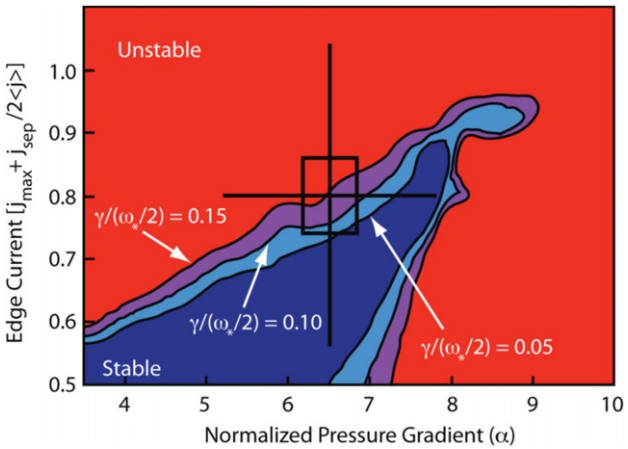

Figure 10. Peeling–ballooning stability diagram as calculated by the ELITE code for shot 135159 during the type-V ELMy phase.

Figure 10 shows the peeling–ballooning stability calculation for the same toroidal modes in the type-V ELMy case. The plasma is still in the unstable region on the peeling side of the stability curve; however, the decreased triangularity (figure 5(*d*)) has decreased the stability to ballooning modes. This results in the appearance of the ballooning boundary on the right-hand side of the figure. The most unstable mode is again $n = 3$, but the operating point is now quite close to the $n = 15$ stability boundary, due to the decreased ballooning stability. Going from the type-I to the type-V case, the operating point makes a lateral transition along the stability boundary. Similar stability calculations for DIII-D show that discharges with the EHO lie near to but on the stable side of the peeling stability boundary [9, 10]. In DIII-D discharges, the operating point moves to decreased edge current and pressure gradient when going from type-I ELMing to QH-mode. This is not the same behaviour as is observed in this pair of NSTX discharges.

4. Summary and discussion

Stabilization of type-I ELMs in NSTX allows transition to a small-ELM operating regime, and is correlated with the presence of an edge instability. The unstable mode has characteristics similar to the EHO, and is localized in the pedestal, but also has significant differences. Density fluctuations due to this instability have been measured, but initial transport modelling is unable to determine if this instability is providing increased edge transport to stabilize the peeling–ballooning modes responsible for type-I ELMs. Reduction in the ion pressure gradient in the pedestal does provide some indirect evidence of increased transport. The observed NSTX mode appears to be resistive in nature, in contrast to the EHO, which is thought to be a saturated ideal kink.

The transition to small-ELMs is also correlated with increased ν^* near the edge. This is in contrast to the QH-mode, which is accessed at decreased ν^*. Comparison of two discharges that have differing ELM characteristics show that the total toroidal edge current is slightly decreased in the type-V ELMing case, but both cases are calculated to be on the unstable side of the peeling boundary with the type-V case having higher pressure gradient. The observed decrease in current is well within experimental error, and is thus not conclusive. Decreased triangularity in the type-V case brings this discharge closer to the ballooning stability boundary than is typically observed in NSTX, though further analysis is required to determine if this change in operating point is related to the stabilization of type-I ELMs. This transition is not the same as that observed for QH-mode, where the operating point clearly moves from the unstable to the stable side of the peeling boundary.

Acknowledgment

This work was supported by US DOE Contracts DE-AC05-00OR22725, DE-FG03-99ER54527, DE-FG03-95ER54309 and DE-AC02-09CH11466.

References

[1] Roth J. *et al* 2009 *J. Nucl. Mater.* **390–391** 1
[2] Ono M. *et al* 1997 *Phys. Plasmas* **4** 1953
[3] Maingi R. *et al* 2005 *Nucl. Fusion* **45** 264
[4] Maingi R. *et al* 2006 *Phys. Plasmas* **13** 092510
[5] Burrell K.H. *et al* 2001 *Phys. Plasmas* **8** 2153
[6] Greenfield C.M. *et al* 2001 *Phys. Rev. Lett.* **86** 4544
[7] Suttrop W. *et al* 2005 *Nucl. Fusion* **45** 721
[8] Sakamoto Y. *et al* 2004 *Plasma Phys. Control. Fusion* **46** A299
[9] Snyder P.B. *et al* 2007 *Nucl. Fusion* **47** 961
[10] Burrell K.H. *et al* 2009 *Phys. Rev. Lett.* **102** 155003
[11] Burrell K.H. *et al* 2009 *Nucl. Fusion* **49** 085024
[12] Stutman D. *et al* 2003 *Rev. Sci. Instrum.* **74** 1982
[13] Burrell K.H. *et al* 2005 *Phys. Plasmas* **12** 056121
[14] Ongena J. *et al* 2008 *Trans. Fusion Sci. Technol.* **53** 367
[15] LeBlanc B.P. *et al* 2003 *Rev. Sci. Instrum.* **74** 1659
[16] Bell R.E. *et al* 2003 *Bull. Am. Phys. Soc.* **48** 217 LP1 25
[17] Osborne T.H. *et al* 2008 *J. Phys. Conf. Ser.* **123** 012014
[18] Lao L.L. *et al* 1985 *Nucl. Fusion* **25** 1611
[19] Groebner R.J. and Osborne T.H. 1998 *Phys. Plasmas* **5** 1800
[20] Sauter O. *et al* 1999 *Phys. Plasmas* **6** 2834
[21] Maingi R. *et al* 2009 *Phys. Rev. Lett.* **103** 075001
[22] Wilson H.R. *et al* 2002 *Phys. Plasmas* **9** 1277
[23] Snyder P.B. *et al* 2002 *Phys. Plasmas* **9** 2037
[24] Grimm R. *et al* 1976 *Methods Comput. Phys.* **16** 253
[25] Snyder P.B. *et al* 2004 *Plasma Phys. Control. Fusion* **46** A131